

# We are IntechOpen, the world's leading publisher of Open Access books Built by scientists, for scientists

6,900

Open access books available

185,000

International authors and editors

200M

Downloads

Our authors are among the

154

Countries delivered to

TOP 1%

most cited scientists

12.2%

Contributors from top 500 universities



WEB OF SCIENCE™

Selection of our books indexed in the Book Citation Index  
in Web of Science™ Core Collection (BKCI)

Interested in publishing with us?  
Contact [book.department@intechopen.com](mailto:book.department@intechopen.com)

Numbers displayed above are based on latest data collected.  
For more information visit [www.intechopen.com](http://www.intechopen.com)



---

# Numerical Simulations of a High-Resolution RANS-FVDM Scheme for the Design of a Gas Turbine Centrifugal Compressor

---

Chellapilla V K N S N Moorthy and Vadapalli Srinivas

Additional information is available at the end of the chapter

<http://dx.doi.org/10.5772/intechopen.72098>

---

## Abstract

The aero-thermodynamic design and performance of a compressor need to conquer many vital challenges like it is a gas-driven turbo-machinery component, involvement of extensive iterative process for the convergence of the design, enormous design complexity due to three-dimensional flow phenomena, and multiflow physics embedded within a dynamic state-of-the-art. In this chapter, a strong attempt is made to address the above-cited technical issues to achieve an optimized design and performance of a centrifugal compressor with backward swept blade profile producing total pressure ratio of 5.4 with an ingested mass flow rate of 5.73 kg/s. A mean-line design methodology was implemented to configure sizing of the compressor. An optimum grid size was well validated by carrying out computational analysis with three different mesh sizes within the same framework. Finally, a detailed three-dimensional numerical simulation was performed using Reynolds-averaged Navier-Stokes equations based on finite volume discretization method (RANS-FVDM) scheme. Consequently, the polytropic efficiency, total-to-total efficiency, stagnation pressure ratio at a fixed rotational speed, and the overall design and aero-thermodynamic performance of the centrifugal compressor are validated.

**Keywords:** numerical simulations, Reynolds-averaged Navier-Stokes equations, finite volume discretization method, compressor design

---

## 1. Introduction

Centrifugal compressors find usage over wide range of propulsion applications and are regarded as one among the key air-breathing propulsive engine components. The cognitive research and development of compressors is directed toward achieving a higher pressure ratio, higher

---

efficiency, and reduced structural weight of compressor and the engine as well. Various compressor stages achieve gradual increase in the stagnation-to-flow pressure contributed by flow diffusion. Energy is added in the rotor blade section, increasing the total pressure and absolute component of flow velocity. Stator blade row diffuses the flow, thus reducing absolute velocity component and elevating static pressure. Blade topology requires adaptation of a cautious design procedure to achieve the designated pressure rise while minimizing aero-thermodynamic losses in order to run and achieve design pressure ratios and design efficiencies.

In this chapter, a strong attempt is made to enumerate the detailed procedure of the centrifugal compressor in Section 2, concepts and basics of Numerical Schemes in Section 3. Further, a case study is discussed in detail in Section 4, the corresponding results and discussions are presented in Section 5. Final conclusions are summarized in Section 6.

## 2. Centrifugal compressor and the basic steps involved in its design

The design of the centrifugal compressor is very difficult due to the reasons like it is a gas-driven turbo-machinery component, involvement of extensive iterative process for the convergence of the design, enormous design complexity due to three-dimensional flow phenomena, and multiframe physics embedded within a dynamic state-of-the-art. Hence, in this article, a detailed procedure for the design is presented based on the design methodology as explained in the literature [1–3]. The basic steps involved in the design of the centrifugal compressor are discussed in detail in the following sections.

### 2.1. Impeller and velocity triangles

Impeller is the main design task during the phase of the compressor design. There are various strategic geometric/design features to be identified and discussed with respect to impeller, its inlet and outlet design. In principal, aerodynamic losses occurring in majority of turbo-machines arise primarily due to the boundary layer growth, its separation on blade profile, and passage surfaces termed as profile losses widely configured under primary losses.

The velocity triangles of the impeller of a centrifugal compressor are diagrammatically shown in **Figure 1**.

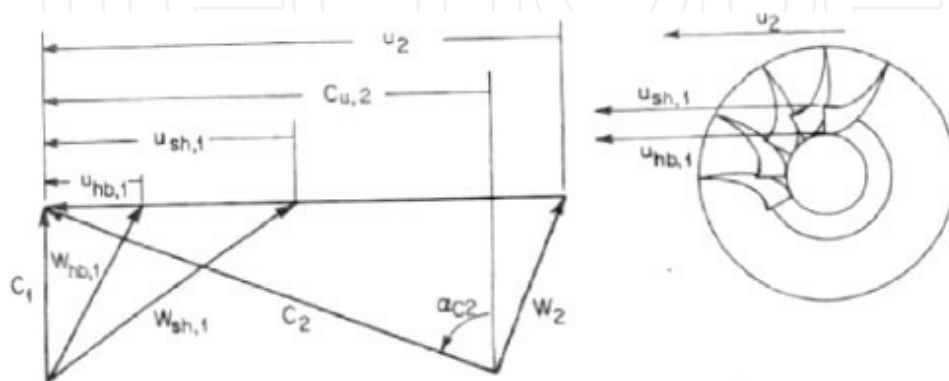


**Figure 1.** Velocity triangles of impeller for a centrifugal compressor.

The impeller design is the basic and major vital part of the design of the compressor. The following conditions for the design may be considered as limiting conditions

1. At the inlet of the impeller, very high relative velocity of the shroud ( $W_{sh,1}$ ) should be avoided.
2. Separation of the flow in the passages of the impeller should be minimized so that the losses are minimized.
3. To meet the above limiting condition, the de Haller impeller ratio should be  $\frac{W_2}{W_{sh,1}} > 0.75$ .
4. The stability of the diffuser strongly depends on  $\alpha_{c,2}$  and for both vaneless and vaned diffusers,  $\alpha_{c,2} \leq 70^\circ$ . Further, it should be taken from  $60$  to  $65^\circ$  for better design.
5. For the backswept impellers, the ratio of the relative velocities should be increased for betterment in the design.
6. Little bit of the increase in the stagnation enthalpy will be attributed to that of the velocity, because of which the polytropic efficiency of impellers with nil back sweep will be less than that of backswept impellers.
7. Work coefficient for radial impellers with zero back sweep is around 0.9 and 0.5 for backswept impellers.
8. To withstand the stress levels, the maximum rotational speed of the backswept impeller is maintained less than that of the radial impeller with same tip diameter.
9. The above two conditions lead to decrease in the maximum possible work per stage for a backswept impellers.
10. Hence, if the maximum work per stage is not required, blade swept angles up to  $50^\circ$  can be used.

## 2.2. Specific work

The specific work can be calculated using the following correlation, which is based on energy and Euler turbine equations

$$(u_2 C_{u,2} - u_1 C_{u,1}) = g_c C_p g T_{0,1} \left\{ \left( \frac{p_{0,2}}{p_{0,1}} \right)^{\left[ \left( \frac{R}{C_p} \right)^{\frac{1}{\eta_{p,c}}} \right]} - 1 \right\} \quad (1)$$

## 2.3. Slip factor

In general for the design of the compressor, the inlet swirl is considered as zero and hence,  $C_{u,1} = 0$ . Furthermore, the Wiesner's correlation for slip factor is given by

$$\sigma_w = \text{slip factor} = \frac{C_{u,2,ac}}{C_{u,2,tl}} = 1 - \frac{\sqrt{\cos \beta_2}}{Z^{0.7}} \quad (2)$$

where number of blades is denoted by  $Z$  and  $\beta_2$  represents the angle between the radial direction and tangent to the rotor blade at the periphery.

$\alpha_{c,2}$  should be less than  $60^\circ$  such that the downstream diffuser does not get prone to stall when  $C_2$  and  $C_{r,2}$  are reduced by keeping very large  $\alpha_{c,2}$ .

## 2.4. Number of blades

The number of blades and the exit blade angle are dependent on each other and can be calculated using loading coefficient. Loading coefficient  $\psi$  is the ratio between the outlet tangential flow velocity and blade speed, which is given by the correlation

$$\psi = \frac{C_{u,2,sc}}{u_2} = \left\{ \left[ \frac{\tan \beta_2}{\tan \alpha_{c,2}} \right] + \frac{1}{\sigma_w} \right\}^{-1} \quad (3)$$

For the sake of easy reference, even number of blades are chosen so that half of the blades can be considered as splitter blades. In general for a better design, 20 blades and  $45^\circ$  blade angle at outlet are taken.

## 2.5. Blade peripheral speed

The peripheral speed of the impeller is calculated using the following correlations

$$-\Delta h_0 = \psi u^2 \quad (4)$$

where increase in the enthalpy is given by

$$\Delta h_0 = C_p (T_{0,2} - T_{0,1}) \quad (5)$$

The isentropic law can be applied, which is given by

$$\frac{T_{0,2}}{T_{0,1}} = \left( \frac{p_{0,2}}{p_{0,1}} \right)^{\left[ \left( \frac{R}{C_p} \right) \frac{1}{\eta_{p,c}} \right]} \quad (6)$$

The polytropic efficiency  $\eta_{p,c}$  can be calculated by choosing isentropic efficiency  $\eta_{s,c}$  as 0.83 and optimum specific speed  $N_s$  as 0.8 for the better design and using the following correlation

$$\eta_{s,c} = \frac{r^{R/C_p - 1}}{r^{(R/C_p) \eta_{p,c} - 1}} \quad (7)$$

Other blade parameters can be calculated using the regular trigonometric correlations from the velocity triangles of the blade like the following

$$C_{u,2,ac} = \psi u_2 \quad (8)$$

$$C_{r,2} = \frac{C_{u,2,ac}}{\tan \alpha_{c,2}} \quad (9)$$

$$C_2 = \frac{C_{u,2,ac}}{\sin \alpha_{c,2}} \quad (10)$$

## 2.6. Density at the inlet of the blade

The Mach number at the inlet can be calculated using the following correlation

$$\frac{C}{\sqrt{g_c R T_0}} = \sqrt{2 \frac{C_p}{R} \left[ 1 - \left[ 1 + \frac{M^2}{2 \left( \frac{C_p}{R} - 1 \right)} \right]^{-1} \right]} \quad (11)$$

Static density can be calculated from the following correlations

$$\frac{\rho_0}{\rho_{st}} = \left[ 1 + \frac{M^2}{2 \left( \frac{C_p}{R} - 1 \right)} \right]^{\left( \frac{C_p}{R} - 1 \right)} \quad (12)$$

## 2.7. Rotational speed

The rotational speed can be calculated using the following correlation

$$N = \frac{60 N_s (g_c \Delta h_0)^{3/4}}{2\pi \sqrt{\dot{V}}} \quad (13)$$

## 2.8. Blade axial width at outlet

The outlet blade axial width is calculated with the assumptions that the effect of the thickness and boundary layer of the blade are neglected. The following correlations are used for the calculations

$$\dot{m} = C_{r,2} \rho_{st,2} \pi d_2 b_2 \quad (14)$$

where,  $d_2$ , the rotor diameter can be calculated using the correlation

$$u_2 = \frac{\pi d_2 N}{60} \quad (15)$$

## 2.9. Flow separation condition

Flow separation should be minimized in the design. To reduce the separation of the flow, the back sweep angle should be higher. Furthermore, the separation in the rotor with subsonic inlet relative Mach number and normal Reynold's number can be minimized by using a lower limit of the ratio of the outlet to inlet velocity ratio as 0.8.

### 3. Numerical schemes

In any gas turbine, the flow of the fluid in the compressor is always more unsteady and turbulent, which further makes the design more complicated. For all turbulent flows, the governing equations are the unsteady Navier-Stokes (N-S) equations. But those equations are very much difficult to solve. The following are the governing equations in tensor notation for understanding the basic nature of the equations as presented by [4].

$$\frac{\partial \rho u_i}{\partial t} + \frac{\partial (\rho u_i u_j)}{\partial x_j} = -\frac{\partial (p)}{\partial x_i} + \frac{\partial}{\partial x_j} \left( \mu \left[ \frac{\partial (u_i)}{\partial x_j} + \frac{\partial (u_j)}{\partial x_i} \right] \right) - \frac{\partial}{\partial x_i} \left( \frac{2}{3} \mu \frac{\partial (u_k)}{\partial x_k} \right) + S_i \quad (16)$$

Energy equation is given by

$$\frac{\partial \rho e}{\partial t} + \frac{\partial (\rho u_j e)}{\partial x_j} = -p \frac{\partial (u_j)}{\partial x_j} + \frac{\partial}{\partial x_j} \left( k \frac{\partial (T)}{\partial x_j} \right) + \Phi + S_i \quad (17)$$

where

$$\Phi = \left( \mu \frac{\partial (u_i)}{\partial x_j} \left[ \frac{\partial (u_i)}{\partial x_j} + \frac{\partial (u_j)}{\partial x_i} \right] \right) - \left( \frac{2}{3} \mu \left( \frac{\partial (u_k)}{\partial x_k} \right)^2 \right) \quad (18)$$

The main disadvantage in solving N-S equations is computing. This is due to the reason that to represent even very small scale of velocity and pressure fluctuations using N-S equations, temporal resolution is required as the N-S equations are spatial fineness equations. Furthermore, the accuracy and resolution of the scheme reduce due to the increase in accumulative rounding off value errors because of the increase in grid points to achieve fine meshes.

Hence, more accurate schemes are required to achieve the solutions of turbulence models with highest resolution. One such numerical scheme, which can effectively solve the turbulence problems, is Reynolds-averaged Navier-Stokes (RANS) equations.

#### 3.1. Reynolds-averaged Navier-Stokes (RANS) equations

The transport equations should be modified by introducing the components with averaged and fluctuating components for solving the turbulent models. RANS are the equations of the motion of the fluid flow with time-averaged equations. If flow turbulence properties are known, then suitable approximations can be made and high-resolution solutions to the N-S equations can be achieved by solving the RANS equations. The RANS equations in tensor notation are described below [4]

$$\rho \frac{\partial \bar{u}_i}{\partial t} + \rho \frac{\partial (\bar{u}_i \bar{u}_j)}{\partial x_j} = \rho \bar{f}_i + \frac{\partial}{\partial x_j} \left( -\bar{p} \delta_{ij} + 2\mu \bar{S}_{ij} - \rho \overline{u'_i u'_j} \right) \quad (19)$$

where  $\bar{S}_{ij} = \frac{\partial (\bar{u}_i)}{\partial x_j} + \frac{\partial (\bar{u}_j)}{\partial x_i}$  is the mean rate of strain tensor.

The problems of physical engineering, which involve high turbulence when modeled based on RANS equations, are also called statistical turbulence models because the method strongly involves statistical averaging procedure. Consequently, the computational effort to solve RANS equations is very less when compared to the other schemes.

### 3.2. Governing equations for turbulence models

As discussed in the earlier articles, due to the involvement of more unknown parameters in the modeling of turbulent problems, the accuracy of the model becomes very much difficult and leads to erroneous results. Hence, it is required to develop a numerical procedure to close or converge the system of equations. One such two equations category turbulence model is K-epsilon model [4].

#### 3.2.1. K-epsilon models

In this model, the velocity of the turbulent flow and the length scales are independently calculated using two different equations. The basic model is the standard k-epsilon model [4].

##### 3.2.1.1. Standard k-ε model

The velocity of the turbulence can be calculated by forming a model for the corresponding kinetic energy using the following Eq. (4)

$$\frac{\partial(\rho k)}{\partial t} + \frac{\partial(\rho k u_i)}{\partial x_i} = \frac{\partial}{\partial x_j} \left[ \left( \mu + \frac{\mu_t}{\sigma_k} \right) \frac{\partial(k)}{\partial x_j} \right] + P_k + P_b - \rho \varepsilon - Y_M + S_k \quad (20)$$

The length scale is represented by  $\varepsilon$ , which is the rate of dissipation and can be calculated from the Eq. (4)

$$\frac{\partial(\rho \varepsilon)}{\partial t} + \frac{\partial(\rho \varepsilon u_i)}{\partial x_i} = \frac{\partial}{\partial x_j} \left[ \left( \mu + \frac{\mu_t}{\sigma_\varepsilon} \right) \frac{\partial(\varepsilon)}{\partial x_j} \right] + C_{1\varepsilon} \frac{\varepsilon}{k} (P_k + C_{3\varepsilon} P_b) - C_{2\varepsilon} \rho \frac{\varepsilon^2}{k} + S_\varepsilon \quad (21)$$

where  $P_k$  represents the turbulence kinetic energy due to the mean velocity gradients,  $P_b$  represents the turbulence kinetic energy due to buoyancy, and  $Y_M$  represents the contribution of the fluctuating dilatation in compressible turbulence to the overall dissipation rate.

### 3.3. Mean: Line analysis

The difficulty in the design of the compressor is because it involves two vital phases of the design. One being the 1D design of the compressor and the other is the deep numerical analysis of the design. The difficulty in the first phase is overcome by using mean line theory. In principle, the mean line theory follows the preliminary design that is carried out by neglecting the air flow variations in radial direction and the location of the mean blade radius is considered for the analysis.

### 3.4. Finite volume discretization method(FVDM)

Any fluid flow problem can be solved with high resolution when the basic concept of continuum is considered during the numerical solution methodology. Finite volume discretization method (FVDM/FVM) is one such methodology developed by McDonald, MacCormack, and Paullay during 1970s. The basic structure of the FVM is as follows:

1. The physical problem is discretized into control volumes.
2. Each control volume is formulated with balance equations involving integrals.
3. Numerical integration is applied to approximate the integral equations.
4. Nodal value interpolations are used to approximate the derivatives and function values.
5. The solution is achieved by assembling the algebraic systems of the discrete control volumes.

## 4. Case study: Design of the centrifugal compressor

The case study presented in the literature [5] is considered for the present illustration for the design and numerical analysis of the centrifugal compressor. Main objective of the current work is to design a centrifugal compressor capable of delivering a pressure ratio of 5.4 with a mass flow ingestion rate of 5.73 kg/sec. The compressor is targeted to achieve 82% total-total efficiency with design constraints of 280 mm for the impeller and 340 mm for the diffuser in terms of diameter. Also, the compressor has to generate flow parameters relative to functional downstream components.

### 4.1. Centrifugal compressor specifications

The input parameters of the centrifugal compressor are tabulated in **Table 1**.

| S. No | Name of the parameter     | Value      |
|-------|---------------------------|------------|
| 1     | Mass flow rate            | 5.73 kg/s  |
| 2     | Pressure ratio            | 5.4:1      |
| 3     | Efficiency                | 82%        |
| 4     | Maximum impeller diameter | 280 mm     |
| 5     | Maximum diffuser diameter | 340 mm     |
| 6     | Rotational speed          | 38,000 rpm |
| 7     | Inlet pressure            | 101,325 Pa |
| 8     | Inlet temperature         | 288.15 K   |

**Table 1.** Geometrical and functional specifications of analysed turbo-machinery.

Preliminary design of the impeller and vaned diffuser is carried out by adapting a one-dimensional model approach. Comprehensive design of the centrifugal compressor stage was generated using ANSYS BladeGen module.

## 4.2. Impeller design

Impeller was designed using guidelines from various sources and in specific from [6]. The number of impeller blade profiles was configured based upon a choice iterative method aiming for passage flow devoid of heavy separations, and it was streamlined and set at 19 blade profiles. A rotational speed of 38,000 rpm was set for the impeller.

### 4.2.1. Impeller inlet

Hub-to-tip ratio is a key owing to the secondary losses, which occurs in the flow regions near the end walls. The presence of any undesirable circulatory or cross-flows develops on account of rapid and steep flow turning through the blade channel accounting for annulus wall boundary layers. Therefore, impeller hub-to-tip ratio was set at 0.35 within the range of 0.3–0.6 prescribed in [6].

Mach number at impeller inlet was set at 0.65. Impeller inlet blade angles were setup by PCA Engineer's Vista CCD tool analytical calculations. The inducer leading edge angles are 35, 56, and 63°, respectively, with incidences of 11.8, 3.7, and 0.1° at hub, mean, and shroud, respectively. Leading edge of the impeller was defined by an elliptic ratio of 6.

### 4.2.2. Impeller outlet

Impeller backswept angle was set at 0° to minimize impeller diameter, and a lean angle of 30° was also incorporated into the design. Impeller exducer height at 13.7032 mm and impeller diameter of 257.954 mm were set by PCA Engineer's Vista CCD software impeller trailing edge that was defined as a square cutoff.

Data generated by Vista CCD tool were used to generate a 3D computer-aided design model of impeller. Inlet portion of 50 mm and horizontal was designed satisfying the diameter constraint of 280 mm.

## 4.3. Design of vaned diffuser

In order to obtain higher pressure ratio in a radial diffuser, the diffusion process has to be achieved across a relatively shorter radial distance. This requires the application of vanes, which provide greater guidance to flow inside diffusing passages. The vaned diffuser was designed by observing various flow parameters reflected at impeller exit after performing numerical simulations.

To circumvent flow separation, divergence of diffuser blade passages in vaned diffuser ring can be kept small by incorporating a large number of vanes. However, this can lead to higher friction losses. Thus, an optimum number of diffuser vanes must be employed and ensure flow passage divergence not to exceed 12°. Thus, final diffuser design contains 30 blades. The

diffuser vane leading edge was at a radius of 136 mm, and the trailing edge of the diffuser vanes was set at a radius of 166 mm. Blade inlets and outlet angle were set at  $64^\circ$ . The leading and trailing edge were defined by an elliptic ratio of 6 and a radius of 0.25 mm.

Another method to prevent very steep velocity gradients at diffuser entry is by providing a small vane-less space ( $0.05d_2-0.1d_2$ ) between impeller exit and diffuser entry. Therefore, a vane-less space of 7.023 mm was allotted.

The design methodology adapted was mainly focused aiming at decrease in Mach number and flow angle at diffuser exit by satisfying a diameter constraint of 340 mm.

#### 4.4. Meshing strategy

Adapted meshing strategy for both the impeller and diffuser fluid domains was achieved using Ansys-Turbo grid module. A total node count of  $7e-01$  million was setup for the CFD solver, as it allows generation of refined quality hexahedral meshes required for the blade passages in turbo-machinery.

#### 4.5. Numerical setup

In the present context, ANSYS tool is setup with pressure-based solver simulating a steady, three-dimensional viscous flow fields using complete set of Navier-Stokes code solving for Reynolds-averaged Navier-Stokes equations based on finite volume discretization method [7]. A high-resolution scheme is used to solve for continuity, momentum, energy, and state equations implementing a standard  $k-\epsilon$  turbulence model. Individual compressor stage characteristics were generated by performing simulations varying back pressures. Firstly, near choke condition, flow points are run to reduce static back pressure values and later, solutions are restarted with incrementally increasing the static back pressure to compute intermediate points on constant speed line running toward stall.

**Inlet boundary conditions:** At compressor inlet, a constant total pressure and total temperature conditions are imposed with a turbulence intensity of 1% and flow direction is marked normal to the inlet plane.

**Outlet boundary conditions:** At the outlet, an average static pressure boundary condition is implemented. Also, a circumferential symmetry condition is imposed on corresponding periodic surfaces with air-fluid medium setup as an ideal gas. A counter-rotating wall boundary is given at the impeller shroud.

### 5. Results and discussions

#### 5.1. Flow analysis: Velocity triangles

Entry and exit velocity triangles for impeller blades along the radial section with backward swept blades ( $\beta_2 = 0^\circ$ ) are plotted as shown in **Figure 2(a)** and **(b)**. Inlet Mach number is

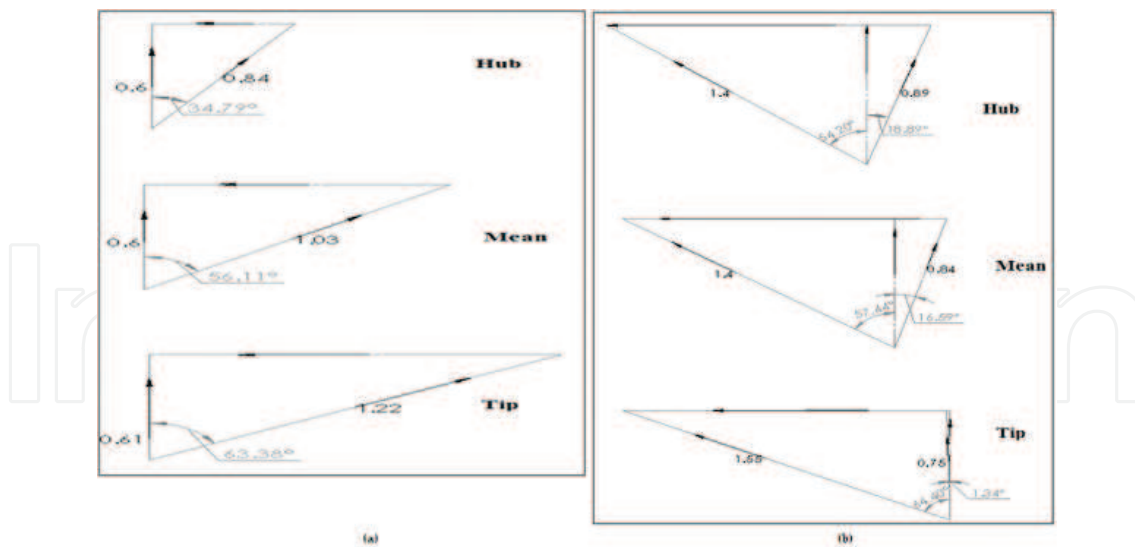


**Figure 2.** (a) Inlet Mach triangles for impeller blades only in radial section with backward swept blades,  $\beta_2 = 0^\circ$  with zero swirl at entry; (b) exit Mach triangles for impeller blades only in radial section with backward swept blades,  $\beta_2 = 0^\circ$  with zero swirl at entry.

within the recommended range of 0.4 to 0.6. A maximum flow angle of  $64^\circ$  at the impeller exit and a Mach number of 1.4 are observed.

## 5.2. Blade to blade contours

Blade to blade contours for absolute Mach number at hub, mean and tip sections are presented in below **Figure 3 (a)** and **(c)**.

The absolute Mach number plots show no supersonic regions of significant volume. The hub section plot show supersonic flow near suction surface of the blade and the tip Section span plots show a supersonic region on the pressure surface of the blade. The presence of a mild bow shock in front of the leading edge of the blade can also be observed. The Mach number is around 0.6 at the leading edge of the impeller. The following plots shown in **Figure 4(a-c)** are the relative Mach number contours for the hub, mean and tip.

The Mach number at the leading edge in the relative frame is near 1.2 for the leading edge of the impeller blade. The regions of low Mach number can also be observed, although it is in the relative frame.

## 5.3. Circumferential contour

Circumferential relative Mach number contours at the impeller inlet and outlet are presented in **Figure 5(a)** and **(b)**. The higher color temperature indicates higher values of relative Mach number.

From above **Figure 5(a)**, corresponding inlet relative Mach number contours shows that passage area is lying in the supersonic regime. The **Figure 5(b)** shows the effect of lean angle of impeller blades.

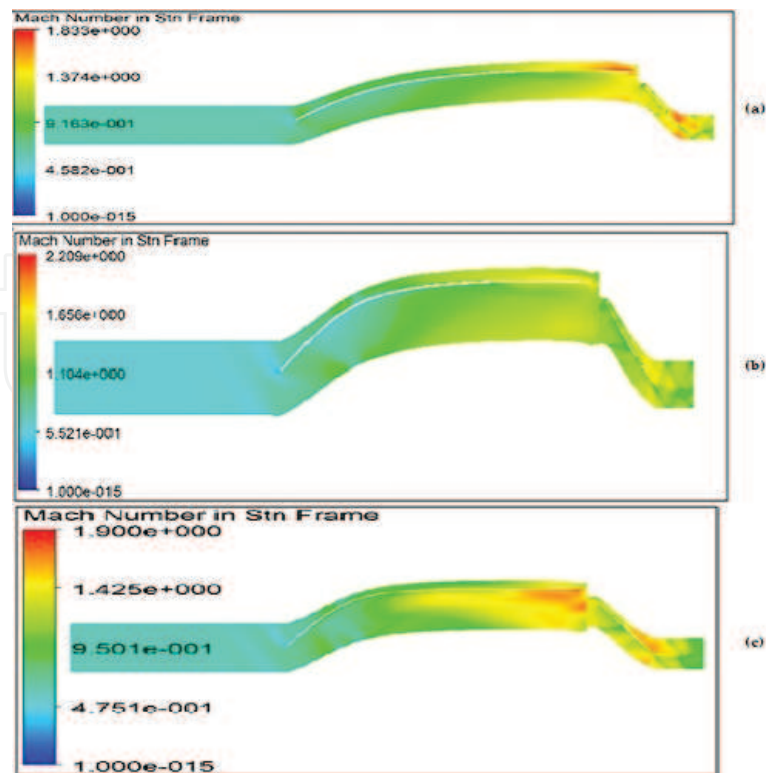


**Figure 3.** (a) Hub section absolute Mach number contour, (b) mean section absolute Mach number contour, and (c) tip section absolute Mach number contour.

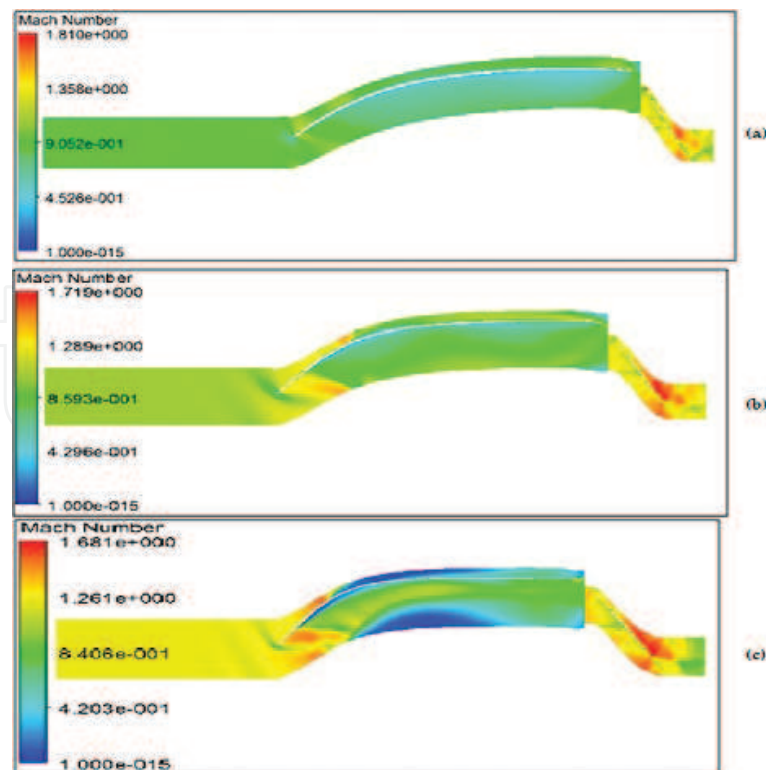


**Figure 4.** (a) Hub section relative Mach number contour, (b) mean section relative Mach number contour, and (c) tip section relative Mach number contour.

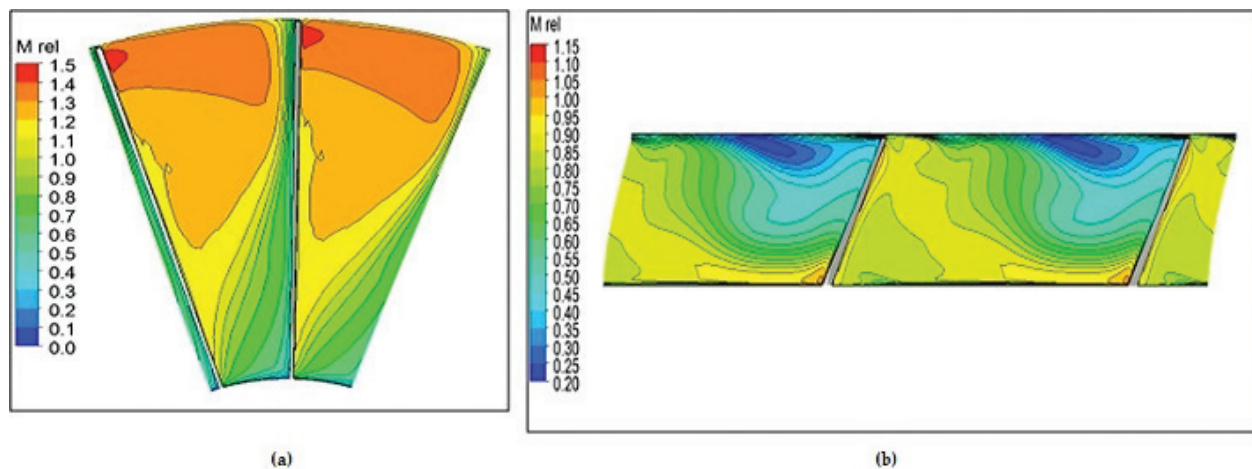


**Figure 5.** (a) Inlet relative Mach contour and (b) outlet relative Mach contour.

## 5.4. Performance characteristics

Individual component as well as stage performance as a whole can be gauged by different methods.

### 5.4.1. Impeller performance characteristics

Impeller performance was evaluated by Vista-CCM and their corresponding plots are shown in below **Figure 6** represents the variation of pressure ratio with varying mass flow ingested through compressor.

**Figure 7** represents the variation of polytropic efficiency with varying mass flow ingested to quantify differential pressure changes occurring through compressor stage.

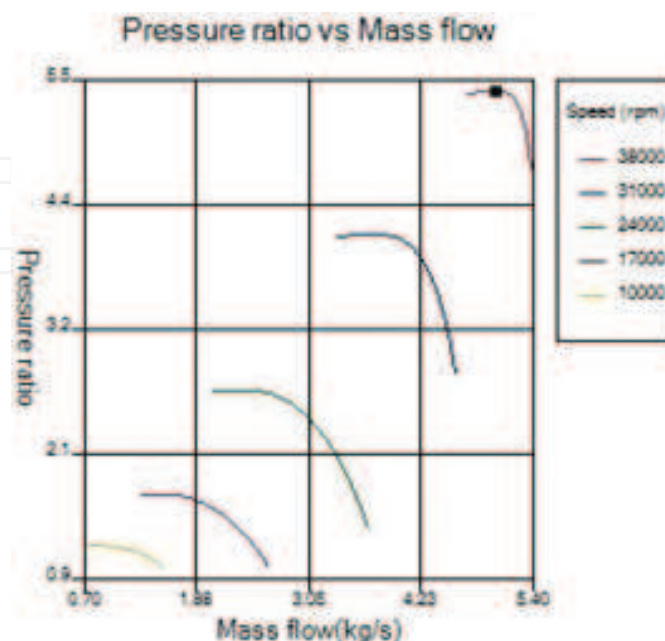


**Figure 6.** Mass flow versus pressure ratio by Vista CCM.

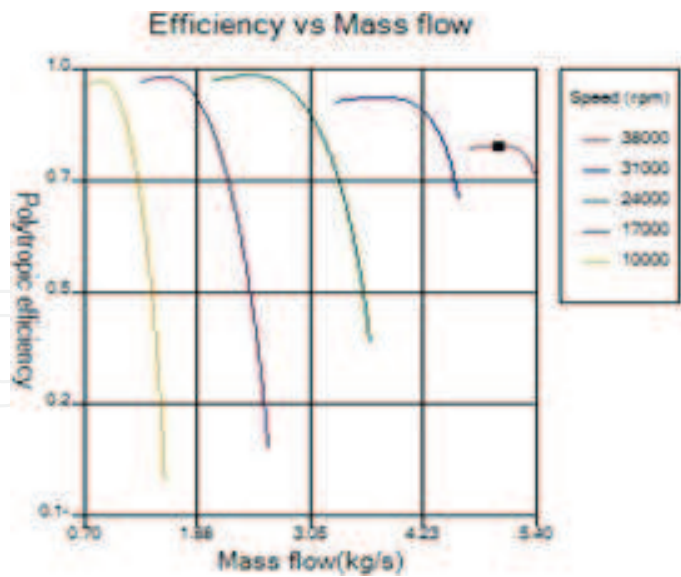


Figure 7. Mass flow versus polytropic efficiency by Vista CCM.

5.4.2. Stage performance characteristics

Compressor stage performance can be evaluated by obtaining individual characteristic curves as plotted in **Figures 8–10**. The compressor performance is presented only for a functional design speed of 38,000 rpm. Variables like total pressure ratio, adiabatic efficiency, and power requirement of compressor are plotted against varying mass flow rate as shown in **Figures 8–10**. The maximum achieved pressure ratio is 5.4 while allowing a fixed mass flow rate of 5.73 kg/s.

A peak efficiency of 75.8% is obtained at a pressure ratio of 5.73. The design point efficiency is predicted to be around 74.5%. Possible reasons for loss in efficiency may be owing to primary and secondary losses.

The impeller works with power a power requirement in the range of 1350–1360 kW on its 100% speed line over the range of total pressure ratio 4.5–5.4.

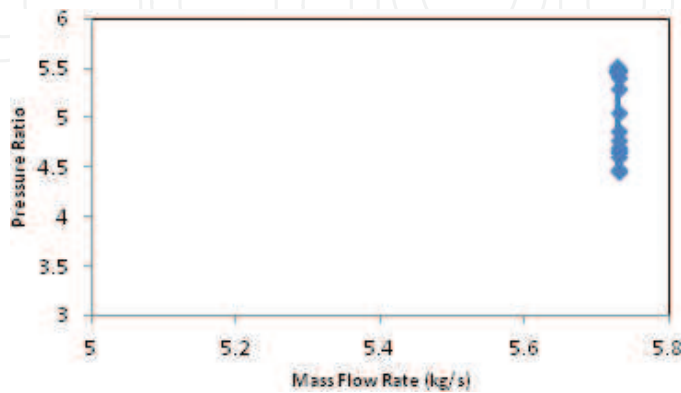


Figure 8. Pressure ratio versus mass flow.

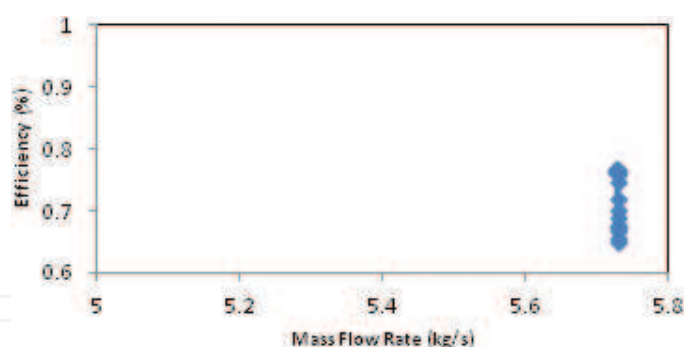


Figure 9. Efficiency versus mass flow.

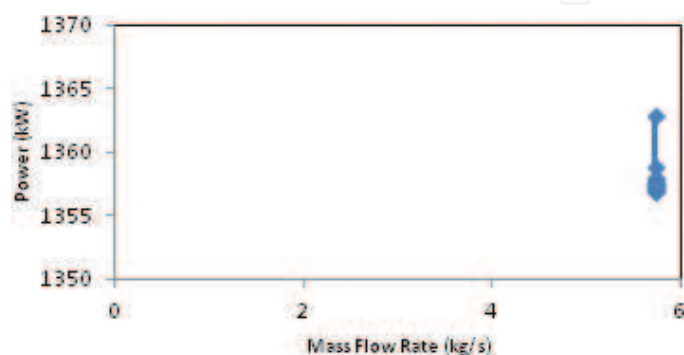


Figure 10. Power versus mass flow.

## 5.5. Validation studies

The obtained results presented in the **Figures 11** and **12** shows state-of-the-art validity of current design with design performance work stated in the literature.

The design methodology adapted in current framework uses a backswept angle of  $0^\circ$  and does not follow the design trend established for validation in above figures. Above deviations in the performance trends can be attributed to the structural size and rotational specifications of various stages.

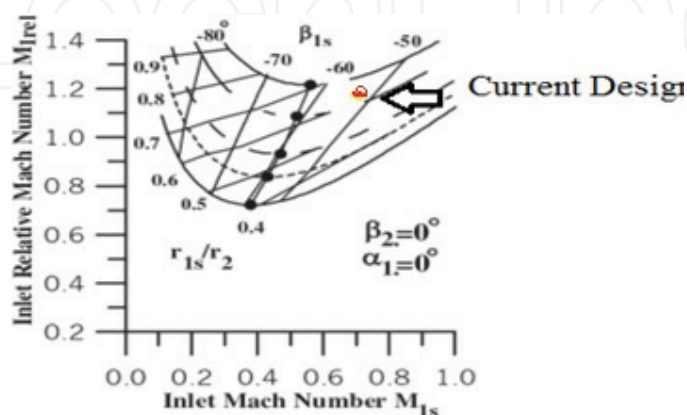


Figure 11. Comparison with compressor in [8].

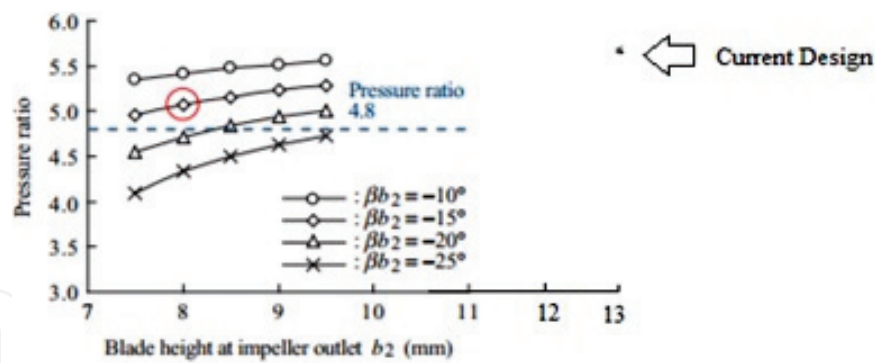


Figure 12. Comparison with trend established in paper [9].

## 6. Conclusion

The aero-thermodynamic design of centrifugal compressor turbo-machinery for a small gas turbine engine has been successfully carried out and sequentially investigated for its performance at design speed. The 3D computational analysis infers that the designed centrifugal compressor generates a pressure ratio of 5.4 with an ingested mass flow rate of 5.73 kg/s at a fixed rotational speed of 38,000 rpm. The targeted flow parameters are in well agreement with centrifugal turbo-machinery within the diameter specification of 280 and 340 mm for impeller and diffuser, respectively. The total-to-total efficiency of designed centrifugal compressor is 81% against a target of 82%. The swirl at impeller is reduced from 77 to 27.5° by the diffuser, thus reducing the primary losses viz., flow separation and thereby has the capability of experiencing lesser stall angles.

## Author details

Chellapilla V K N S N Moorthy<sup>1\*</sup> and Vadapalli Srinivas<sup>2</sup>

\*Address all correspondence to: krishna.turbo@gmail.com

1 Institute of Aeronautical Engineering, Hyderabad, Telangana, India

2 GITAM University, Vishakhapatnam, Andhra Pradesh, India

## References

- [1] Rohlik HE. Radial inflow turbines (in turbine design and application). NASA Special Publication SP 290. 1975;3:31-58
- [2] Rodgers C. Specific speed and efficiency of centrifugal impellers. In: Performance Prediction of Centrifugal Pumps and Compressors. New York: ASME; 1980. pp. 592-603

- [3] Wilson DG, Korakianitis TH. The Design of High Efficiency Turbomachinery and Gas Turbines. 2<sup>nd</sup> ed. New Jersey, United States: Prentice Hall; 2014
- [4] Srinivasa Rao P: Modeling of turbulent flows and boundary layer. In: Hyoung Woo Oh, editor. Computational Fluid Dynamics. London, United Kingdom: InTech; 2010. p. 285-306. ISBN: 978-953-7619-59-6
- [5] Moorthy CHVKNSN, Bharadwajan K, Srinivas V. Computational studies on aerothermodynamic design and performance of centrifugal turbo-machinery. International Journal of Mechanical Engineering and Technology. 2017;8(5):320-333
- [6] Philip P Walsh, Fletcher P. Gas Turbine Performance. 2<sup>nd</sup> ed. Oxford: John Wiley & Sons; 1998. p. 178-186
- [7] Moorthy CHVKNSN, Srinivas V, Prasad VVSH. Computational analysis of a CD nozzle with 'SED' for a rocket air ejector in space applications. International Journal of Mechanical and Production Engineering Research and Development. 2017;7(1):53-60
- [8] Zahed AH, Bayomi NN. Design procedure of centrifugal compressors. ISESCO Journal of Science and Technology. 2014;10(17):77-91
- [9] Hideaki T, Masaru U, Hirata KT. Aerodynamic design of centrifugal compressor for AT14 turbocharger. IHI Engineering Review. 2010;43(2):70-76

